# Chapter 5

# Polar particles induce strings in liquid crystal

## 5.1 Introduction

In the previous chapters, the collective behaviour of active self-propelled particles are explored in different external environment. In this chapter we focus our study on a mixture of polar and apolar particles, both individually are in equilibrium. But mixture is such that one prefers to be in the ordered state and another in the disordered state. Our system consists of liquid crystal in the presence of few polar impurities. Liquid crystal systems have been studied extensively over the years. It is well established that these systems exhibit topological defects. For nematic symmetry of the particles, the stable topological defects have charge $\pm\frac{1}{2}$, which move diffusively through the system and annihilate during the evolution of the system towards the steady state [Chandrasekhar (1992); de1 (1993)]. These defects are also present when the system is active, i.e., "Active nematic" [Doostmohammadi et al. (2018); Giomi et al. (2014); Kumar & Mishra (2020b); Mishra (2014); Mishra et al. (2014); Thampi & Yeomans (2016); Thampi et al. (2014)]. The presence of external particles can significantly influence the dynamics and ordering in active systems. There are several studies in which foreign particles like bacteria are present in the liquid crystal [Amiri et al. (2022); Genkin et al. (2017); Mushenheim et al. (2014); Sokolov et al. (2015); Turiv et al. (2013); Vats et al. (2023); Zhou et al. (2014, 2017)] as well as in Active nematic [Ngo et al. (2012)]. These systems show interesting features like formation of unique structures and dynamics which are absent in the pure systems. Keeping these systems in mind, we want to explore the effect of external passive particles in two dimensional liquid crystal system. We study this system using a coarse-grained

approach in which we write dynamical equations for the slow variables i.e. density and broken symmetry variable like orientation order parameter.

In our study, we couple the liquid crystal with external particles present in it, which are head tail assymetric. Hence backgorund liquid crystal is apolar in nature while external particles are polar in nature. Both the polar and apolar particles are modeled using the time Dependent Ginzburg-Landau (TDGL) equation. We study by assuming external particles to be passive and present in small numbers, e.g., a few polar particles present in the liquid crystal. In this coarse-grained model, the polar particles is in a disordered state, and the average density of the apolar particles is chosen in such a way that it is in the ordered state. We focus our study on the behavior of topological defects formed in the liquid crystal during the evolution of the system starting from the disordered configuration of both liquid crystal and polar particles. This kind of system have been previously studied using spin based microscopic models where interaction of each spin with its neighbor consists of polar and nematic components simultaneously [Lee & Grinstein (1985); Mondal et al. (2024)]. The relative strength of the two types of interaction dictates the kinetics and steady state behaviour of the system. In our model, we have a mixture of two types of particles with distinct symmetry. We introduce a coupling term in the free energy of the mixed system to account for the interaction between the two particles.

Our key observations are as follows: 1.) If coupling strength is larger than a critical value, we observe the formation of strings connecting two defects irrespective of their charge; 2.) The width of string is decreasing and probability of connecting the same type of defect is increasing with the increase of coupling strength and the density of polar particles and 3.) dynamics of $\pm\frac{1}{2}$ defect is enhanced in response to coupling.

## 5.2 Model and Numerical Methodology

We model the polar particles and liquid crystal using coarse-grained free energy and TDGL equations for the slow variables, i.e., the orientation order parameter: polarization $\vec{P}$ for polar particles and tensorial order parameter $Q$ for apolar particles.

**Free Energy Functional of the Pure Polar System:**

$$F_P = \int \bar{dr} \left[ \frac{\alpha_p(\rho_{p_0})}{2} |\vec{P}|^2 + \frac{\beta_p}{4} |\vec{P}|^4 + \frac{\kappa_p}{2} (\partial_i P_j)(\partial_i P_j) \right] \tag{5.1}$$

where the coefficient $\alpha_p(\rho_{p_0}) = \alpha_0 \left(1 - \frac{\rho_{p_0}}{\rho_{pc}}\right)$ is responsible for the order-disorder transition, $\rho_{pc}$ is the critical density, and $\rho_{p_0}$ is the average density of the polar particles. The polar particles are in the homogeneous ordered phase for $\alpha_p < 0$ and in the disordered

phase for $\alpha_p > 0$. The coefficient $\beta_p > 0$ maintains the stability of the system. The third term accounts for the distortion in $\vec{P}$, here, $\kappa_p$ is the elastic constant, taken to be the same for bend and splay distortions.

**Free Energy Functional of the Pure Apolar System:**

$$F_Q = \int \bar{dr} \left[ \frac{\alpha_Q(\rho_{a_0})}{2} Q : Q + \frac{\beta_Q}{4} (Q : Q)^2 + \frac{\kappa_Q}{2} (\vec{\nabla} \cdot Q)^2 \right] \tag{5.2}$$

where the coefficient $\alpha_Q(\rho_{a_0}) = \alpha_0 \left(1 - \frac{\rho_{a_0}}{\rho_{Qc}}\right)$ is responsible for the order-disorder transition, $\rho_{Qc}$ is the critical density, and $\rho_{a_0}$ is the average density of the apolar particles. The apolar particles are in the homogeneous ordered phase for $\alpha_Q < 0$ and in the disordered phase for $\alpha_Q > 0$. The coefficient $\beta_Q > 0$ maintains the stability of the system. The third term accounts for the distortion in $Q$. Here, $\kappa_Q$ is the elastic constant. For convinience, we take $\kappa_P = \kappa_Q = \kappa$.

Because of their elongated shape, polar molecules prefer to align along the direction of the long axis of the liquid crystal and vice versa. Thus, we introduce a coupling term of the form $(Q : \vec{P}\vec{P})$ in the free energy of the mixed system.

**Free Energy for the Mixed System:**

$$F_m = F_P + F_Q + \int d\vec{r} \gamma_1 (Q : \vec{P}\vec{P}) \tag{5.3}$$

Using the free energy in Eq.(5.3), we can write the dynamical equations for Order Parameter

$$\partial_t \vec{P} = -\Gamma_P \frac{\delta F_m}{\delta \vec{P}} + \zeta_P \tag{5.4}$$

$$\partial_t Q = -\Gamma_Q \frac{\delta F_m}{\delta Q} + \zeta_Q \tag{5.5}$$

The term on the left-hand side (L.H.S.) of Eq.(5.4) and Eq.(5.5) represents the time derivative of the polarization vector $\vec{P}$ and the tensorial order parameter $Q$ respectively, indicating how these order parameters evolve over time. On the right-hand side (R.H.S.), $\Gamma_P$ and $\Gamma_Q$ are the kinetic coefficients (or mobilities) associated with the polarization $\vec{P}$ and the tensorial order parameter $Q$, respectively. $\frac{\delta F_m}{\delta \vec{P}}$ and $\frac{\delta F_m}{\delta Q}$ are the functional derivatives of the mixed free energy $F_m$ with respect to $\vec{P}$ and $Q$, respectively. These terms drive the system towards minimizing the free energy $F_m$. The last terms $\zeta_P$ and $\zeta_Q$ account for thermal fluctuations and random perturbations in the polarization and the nematic order parameter in the form of Gaussian white noise having a mean of zero $\langle \zeta_{P,Q}(r,t) \rangle = 0$

and being uncorrelated in time $\langle \zeta_{P,Q}(r,t)\zeta_{P,Q}(r',t')\rangle = \eta_{P,Q}\delta_{P,Q}(r-r')\delta_{P,Q}(t-t')$, with a variance $\eta_{P,Q}$ that is often related to the temperature of the system. In this study, the strength of noise in Eq.(5.4) and Eq.(5.5) is taken as same i.e. $\eta_P = \eta_Q$.

We study the system in two dimensions, which allows us to explore the fundamental behaviors of the system while simplifying the complexity of three-dimensional interactions. In this two-dimensional framework, the dynamics of both the polarization $\vec{P}$ and the tensorial order parameter $Q$ can be analyzed more effectively, providing insight into the structure and ordering of the system. The intrinsic time scale $\tau = \frac{1}{\alpha_0} = 1$ and intrinsic length $l_0 = \sqrt{\kappa\tau}$. The length and time scales in system are re-scaled in terms of $l_0$ and $\tau$ respectively, such that all the terms in the equation become dimensionless. The rescaled equations for the two components of polarization ($P_x$ and $P_y$) and the apolar order parameters ($Q_{xx}$ and $Q_{xy}$) are as follows:

- **Equation for $P_x$:**

$$\partial_t P_x = \left[\alpha_p(\rho_{p_0}) - (P_x^2 + P_y^2)\right] P_x + (\partial_x^2 + \partial_y^2)P_x + \gamma(2P_xQ_{xx} + 2P_yQ_{xy}) + \xi_{P_x} \quad (5.6)$$

- **Equation for $P_y$:**

$$\partial_t P_y = \left[\alpha_p(\rho_{p_0}) - (P_x^2 + P_y^2)\right] P_y + (\partial_x^2 + \partial_y^2)P_y + \gamma(-2P_yQ_{xx} + 2P_xQ_{xy}) + \xi_{P_y} \quad (5.7)$$

- **Equation for $Q_{xx}$:**

$$\partial_t Q_{xx} = \left[\alpha_Q(\rho_{a_0}) - 2(Q_{xx}^2 + Q_{yy}^2)\right] Q_{xx} + \nabla^2 Q_{xx} + \gamma(P_x^2 - P_y^2) + \xi_{Q_{xx}} \quad (5.8)$$

- **Equation for $Q_{xy}$:**

$$\partial_t Q_{xy} = \left[\alpha_Q(\rho_{a_0}) - 2(Q_{xx}^2 + Q_{yy}^2)\right] Q_{xy} + \nabla^2 Q_{xy} + \gamma(2P_xP_y) + \xi_{Q_{xy}} \quad (5.9)$$

In the right-hand side of Eqs. 5.6 to 5.9: The first term represents the mean-field transition, which captures the intrinsic dynamics of the order parameters. The second term corresponds to diffusion, accounting for spatial variations in the $\vec{P}$ and $Q$. The third term introduces the effect of coupling in the system with rescaled coupling strength $\gamma$, which describes the interaction between the polar and the apolar order parameter. The last term represents the contribution of noise $\xi's = \eta\,\delta(r-r')\delta(t-t')$ with strength $\eta$, accounting for thermal fluctuations and random perturbations. The Eqs. 5.6 to 5.9 are written in

rescaled space, such that coefficient of first two terms are set to 1, simplifying the analysis and allowing us to focus on the essential properties driven by the term.

## 5.3 Numerical Details

We simulate the equations (Eq.(5.6) to (5.9)) using the Euler integration scheme on a square lattice of size $L \times L$ with periodic boundary conditions in both the directions. The Euler discretization scheme is applied with mesh sizes $\Delta x = \Delta y = 0.5 l_0 = 0.5$ and time step $\Delta t = 0.01\tau = 0.01$. The spatial discretization ensures that coarsening interfaces are treated smoothly, while the temporal discretization is selected to maintain the stability of the numerical scheme. One simulation step covers $\Delta t$ time.

The system is initialized from a randomized and homogeneous state of apolar particles with an average apolar density $\rho_{a_0} = 0.75$ and critical densities $\rho_{pc} = \rho_{Qc} = 0.5$. The value of $\rho_{a_0}$ is chosen such that the apolar particles are in the ordered phase. Simulations are conducted on a system of size $L = 256$. The strength of the noise $\eta$ is set to 0.1. The average density of polar particles $\rho_{p_0}$ and the coupling strength $\gamma$ are the primary control parameters throughout the study. $\rho_{p_0}$ is varied to ensure that $\rho_{p_0} \ll \rho_{pc}$ keeps the polar particles in the disordered phase, while $\gamma$ is varied in the range $[0, 1]$.

## 5.4 Results

In this study, we investigate the effect of coupling on the structure formation and dynamics within the system. Our primary objective is to observe the time evolution of the polarization vector field $\vec{P}$ and the nematic order parameter field $Q$, as governed by Eqs. 5.6 to 5.9. This analysis is conducted by varying key parameters, specifically the coupling strength $\gamma$ and the average polar density $\rho_{p0}$.

Fig.[5.1] illustrates the temporal evolution of the nematic order parameter field $Q$ (top panel) and the polarization order parameter field $\vec{P}$ (bottom panel) for different values of the coupling strength $\gamma$. The rows (a-e), (f-j), (k-o), and (p-t) correspond to $\gamma = 0$, 0.40, 0.80, and 1.0, respectively. These sequences demonstrate how both fields evolve over time as the coupling strength increases.

For $\gamma = 0$, where the polar and nematic fields are uncoupled, Fig.[5.1](a-e) shows the formation of oppositely charged $\pm\frac{1}{2}$ defects with homogeneous ordering in the background of the $Q$ field. These defects are dynamic, gradually annihilating with oppositely charged counterparts over time. Meanwhile, the corresponding $\vec{P}$ field remains in a disordered phase. This behavior is a direct result of the initial conditions, where $\rho_{a0} > \rho_c$ and $\rho_{p0} < \rho_c$.

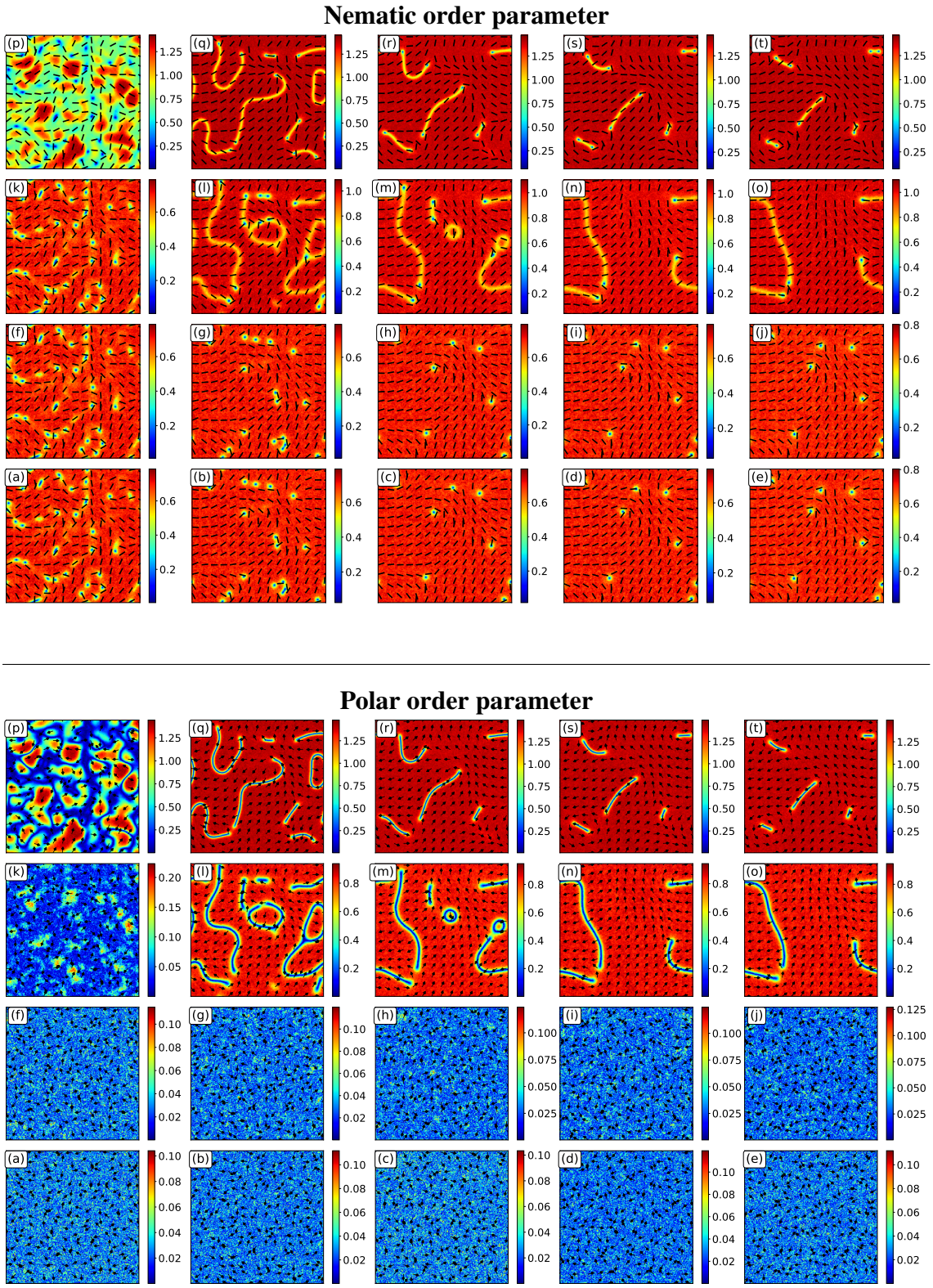


Fig. 5.1 Visualization of the **Nematic order parameter** as $\gamma$ varies from bottom to top and time progresses from left to right. Each row represents a different value of $\gamma$: (a-e)$\gamma = 0$, (f-j) $\gamma = 0.40$, (k-o) $\gamma = 0.80$, and (p-t) $\gamma = 1.00$. The progression from left to right in each row illustrates the temporal evolution (time steps: 1, 8000, 16000, 24000 and 30000) of the Nematic order parameter within each $\gamma$ condition. The same description is valid for the **Polar order parameter**.

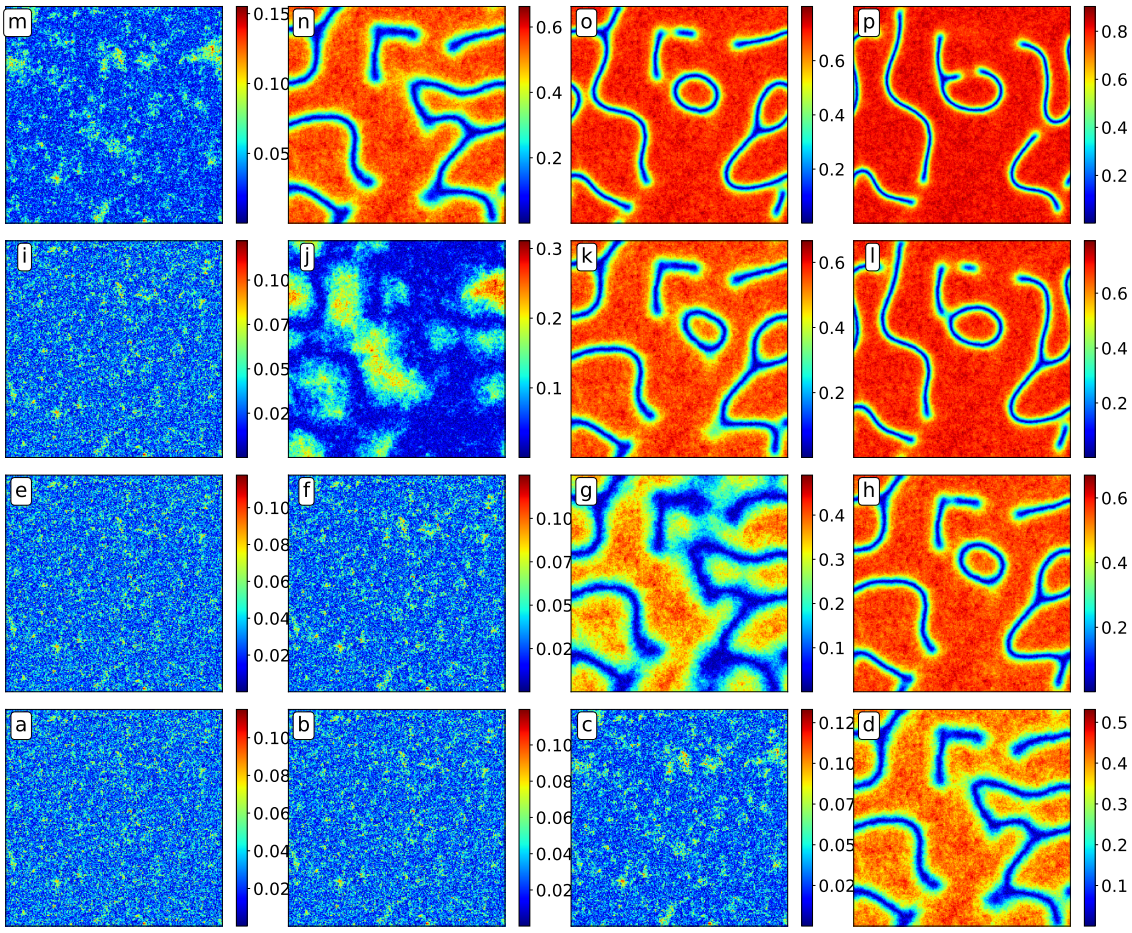


Fig. 5.2 Snapshots of the polar order parameter at a fixed time step i.e. 10000 showing variations in the average density of polar particles from left to right ($\rho_{p0} = 0.05, 0.10, 0.15$ and 0.20) and the coupling strength from bottom to top ($\gamma = 0.50, 0.55, 0.60$ and 0.65).

A similar pattern is observed for $\gamma = 0.40$ in Fig.[5.1](f-j). However, as the coupling strength increases, particularly for $\gamma = 0.80$ and 1.0, distinct structures emerge in the order parameter field which we describe as strings connecting two defects, irrespective of their charge. These strings are visible in both the $Q$ and $\vec{P}$ fields. In the polarization order parameter field, the magnitude of the order parameter approaches zero along the string, which acts as a domain wall separating two oppositely oriented domains of polar particles. In other regions, the magnitude nears one, indicating ordering in the $\vec{P}$ field. The corresponding snapshots for the nematic field show that the magnitude of $Q$ lies between the values at the core of the defect and in the ordered phase. As the system evolves and all defects annihilate, the strings disappear, leading to homogeneous nematic ordering, which in turn induces ordering in the $\vec{P}$ field due to strong alignment at higher coupling strengths.

Fig.[5.2] further demonstrates that a optimal value of $\gamma$ is required for string formation as the average density of polar particles $\rho_{p0}$ increases. This figure presents snapshots of the polar order parameter at a fixed time, with variations in the density of polar particles shown from top to bottom and changes in the coupling parameter depicted from left to right. Each row in Fig.[5.2] corresponds to a different density of polar particles, decreasing from top to bottom, while each column represents a different coupling parameter, ranging from weak to strong coupling. This phase diagram in Fig.[5.2] clearly illustrates how both the density of polar particles and the coupling strength influence the formation of strings and the overall ordering in the $\vec{P}$ field.

Next, we characterize the width of the strings, which is strongly influenced by the density of polar particles and the coupling strength, as shown in Fig.[5.3]. The width is determined by counting the number of sites where the order parameter satisfies $|Q| < 0.2$ along both the $x$ and $y$ directions, and then taking the average of these values. To ensure accuracy, this averaging is performed over several locations in the system. Fig.[5.3] presents a phase diagram illustrating the width of strings formed between pairs of defects as a function of density and the coupling parameter. The color map represents the width of the strings, providing a visual representation of how these properties change with varying conditions. Snapshots of the polar order parameter field in Fig.[5.3] further illustrate the variations in string width with respect to different density and coupling parameters. Each panel corresponds to a different combination of these values: (a) Low density and weak coupling; (b)-(e) Moderate density and moderate coupling; (f) High density and strong coupling.

Our results indicate that higher densities of polar particles and stronger coupling strengths lead to narrower strings. This finding underscores the significant role that these parameters play in determining the structural properties of the system.

Interestingly, we observe that defect pairs connected by strings can be of the same type, such as $(+1/2,+1/2)$ or $(-1/2,-1/2)$, as well as of opposite types, such as $(+1/2,-1/2)$. The probability of strings connecting defects of the same type, $P(\text{same})$, is plotted against the coupling strength $\gamma$ in Fig.[5.4]. Different curves in the figure represent various densities of polar particles.

The probability $P(\text{same})$ is calculated by manually counting how many defects are connected to like pairs and how many to opposite pairs. These counts are then averaged over 40 ensembles to ensure statistical significance.

As the coupling strength $\gamma$ and the average density of polar particles $\rho_{p0}$ increase, the system exhibits a stronger polar behavior, which in turn enhances the likelihood of string formation between like defects. Specifically, pairs of similar half-integer topological

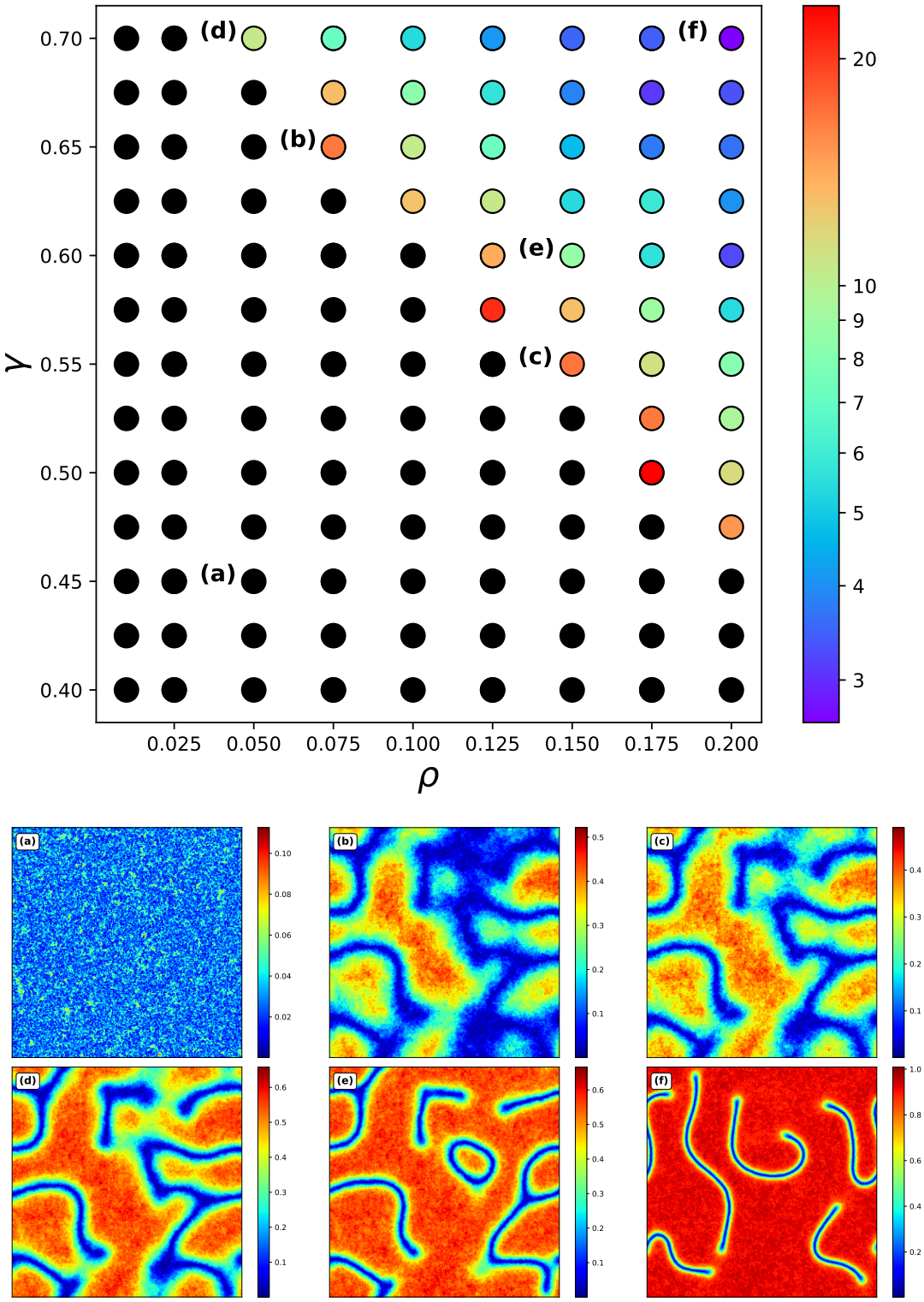


Fig. 5.3 Phase diagram illustrating the width of strings formed between pairs of defects as a function of density and coupling parameter. The color map represents the width of the strings. Snapshots of the polar order parameter field illustrate variations in the width of the strings with respect to density and coupling parameters. Each panel corresponds to a different combination of density and coupling values: (a) Low density and weak coupling; (b)-(e) low density and strong coupling; (f) High density and strong coupling.

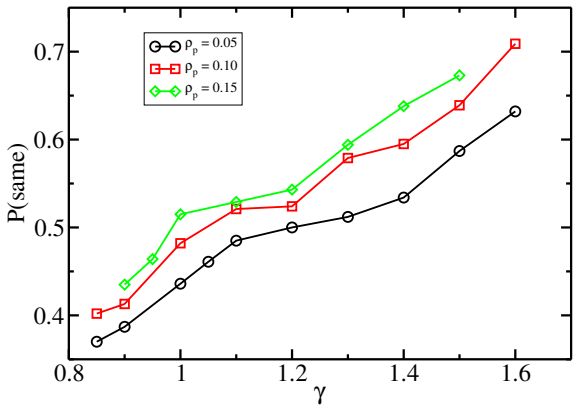


Fig. 5.4 Probability of strings connecting defects of the same nature. Different curves represent different values of density.

defects, such as two $(+1/2,+1/2)$ "comet"-like structures or two $(-1/2,-1/2)$ "triangle"-like structures, are more likely to be connected by strings. These structures effectively behave as full-integer composite defects of $+1$ and $-1$ types, respectively. These composite defects are identified as "aster"-like and "square"-like structures in the literature [Amiri et al. (2022)]. This behavior is prominently visible in Fig.[5.1](r) to [5.1](t).
Next, we discuss the dynamics of the defects in the coupled system. To study the trajectory and dynamics of the system, we have introduced a pair of artificial $\pm\frac{1}{2}$ defects into the coupled system. Since the interaction among the defects plays a crucial role in the dynamics of the defects, it becomes challenging to explicitly observe the effect of coupling on the dynamics. However, by carefully analyzing the trajectories, we can infer the influence of the coupling strength on defect motion and interactions.

### 5.4.1 Artificial Defects in Coupled System

The artificial defects are designed as: Let $(x_1,y_1)$ and $(x_2,y_2)$ are the location of defect cores, then the orientation of the nematic particles at position $(x,y)$ is given by

$$\theta(\vec{r}) = \left[ S\arctan\left(\frac{y-y_1}{x-x_1}\right) - S\arctan\left(\frac{y-y_2}{x-x_2}\right)\right] + \theta_0 \tag{5.10}$$

where, $\theta_0 = 0$ is the orientation far away from the defects such that nematic particles are aligned parallel to the horizontal axis and $S = \frac{1}{2}$ is the topological charge of the defect [Missaoui et al. (2020)]. We chose $(x_1,y_1) \equiv (\frac{L}{4},\frac{L}{2})$ and $(x_2,y_2) \equiv (\frac{3L}{4},\frac{L}{2})$ and the orientation of the defects are chosen such that the head of the $+\frac{1}{2}$ defect is facing the $-\frac{1}{2}$ as shown in Fig.[5.5](a).

We show the snapshots of the system with two kinds of initial configurations: 1.) ordering of polar particles is considered random and 2.) the polar particles are oriented parallel to the direction of positive half defect. The trajectory of artificial defects is shown in the snapshots for $\gamma = 0$ and $\gamma = 1.0$.

- **Random Initial Condition:** For $\gamma = 0$, there is no string formation and the defects move towards each other along the shortest path as shown in Fig.[5.5](a-c). For $\gamma = 1.0$, string is formed in the system which dictates the trajectory of the defects can be seen in Fig.[5.5](d-f).

- **Polar Order Initial Condition:** For $\gamma = 0$, the system shows the same behaviour as for random initial conditions. However, for $\gamma = 1.0$, a well-defined string is formed along the line connecting the defect cores in Fig.[5.5](g-l).

Further, we study the effect of coupling on the dynamics of the defects for both the initial conditions.

The mean square displacement (MSD) of defects is calculated for polar ordered initial conditions at $\gamma = 0$ and $\gamma = 1.0$. The MSD analysis provides quantitative information on the mobility and diffusion behavior of the defects in presence of coupling. We observe enhanced dynamics of the defects for higher coupling strength $\gamma$ as shown in Fig.[5.6].

### 5.4.2 Confined System

We have switched off the noise in the system and applied perpendicular anchoring in polar and nematic on the top and bottom with hard boundary in a rectangular geometry $L \times D$, $(D < L)$. Along x-direction, we have applied periodic boundary condition. We have shown initial condition in Fig.[5.7].

We investigate the formation of wall in the polar order parameter field under the influence of coupling. To determine the width of the wall along the y-axis $(1 - D)$, we compute the one-dimensional polar order parameter, denoted as $P'$, by averaging along the x-axis over the range $(1 - L)$ for each point on the y-axis. Specifically, we assess the width $W$ by counting all points along the y-axis where $P'$ is less than 0.2. If $P' < 0.2$ at a given point along the y-axis, we include that point in the width calculation. Now we characterize the variation of $W$ with respect to $\gamma$ for different average densities of polar particles $\rho_p$ . We have calculated the width of wall and plotted $\frac{W}{D}$ vs. $\gamma$ for $\rho_{p0} = 0.05, 0.10$ and $0.15$ in Fig.[5.8].

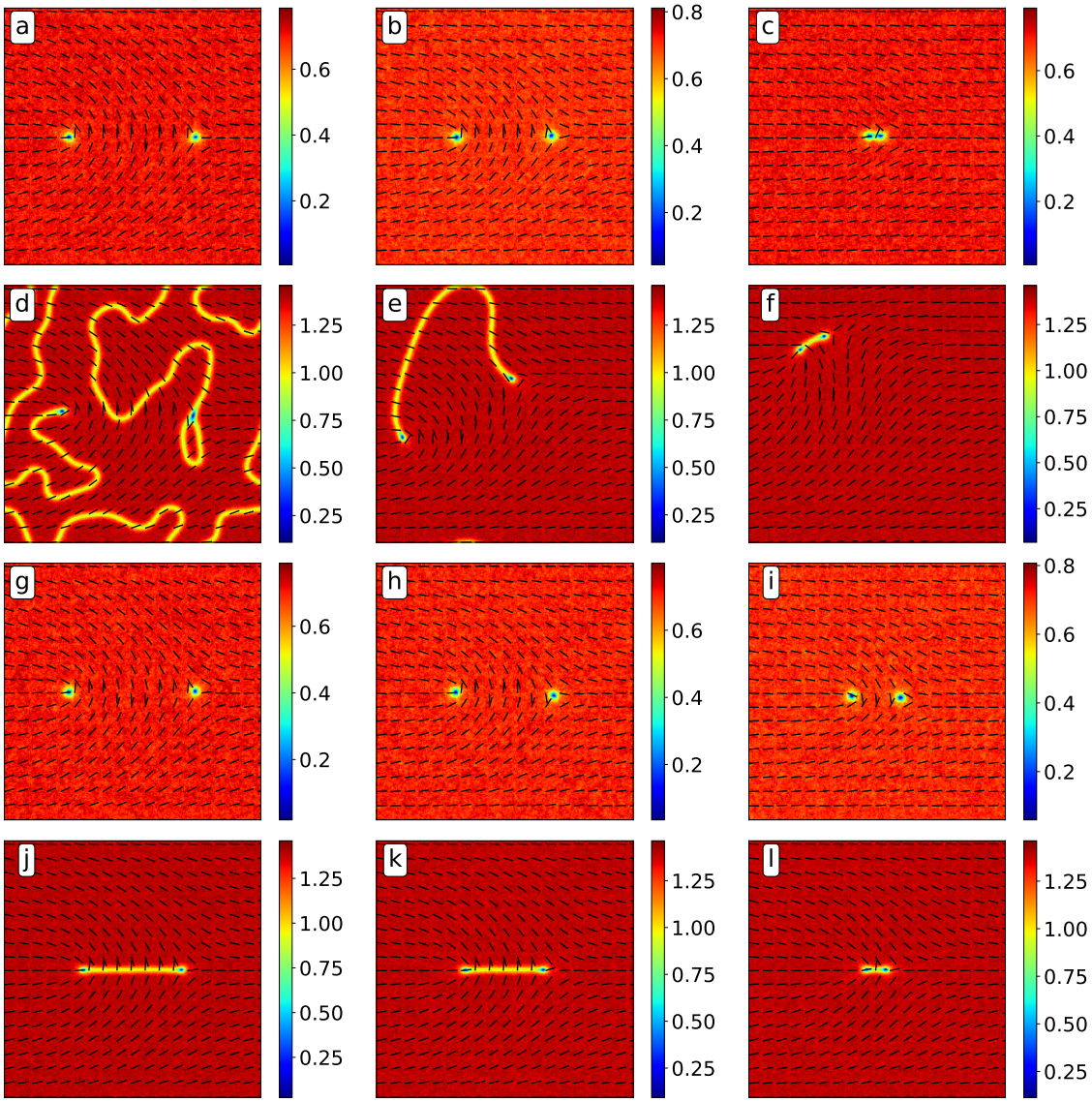


Fig. 5.5 Snapshots for random and polar order initial conditions of polar particles for $\gamma = 0$ and $\gamma = 1.0$.

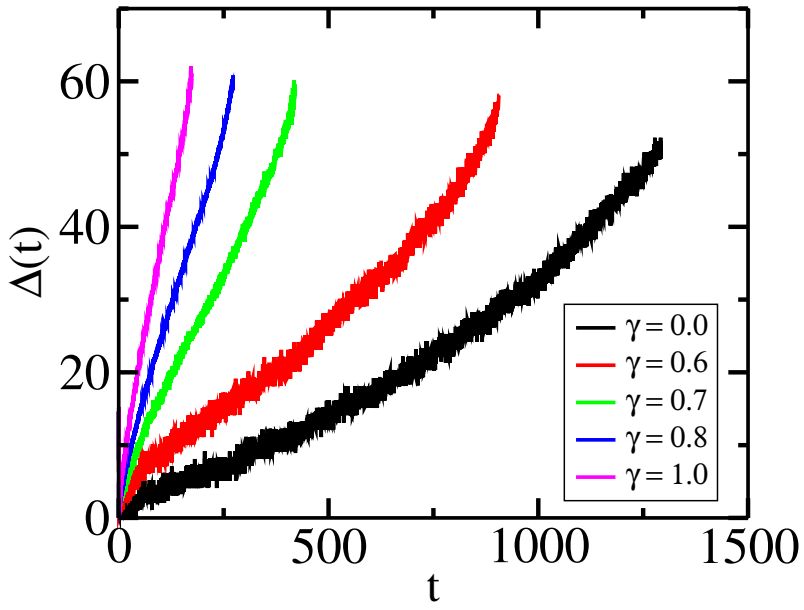


Fig. 5.6 Mean square displacement for random and polar order initial conditions of polar particles from $\gamma = 0$ to $\gamma = 1.0$.

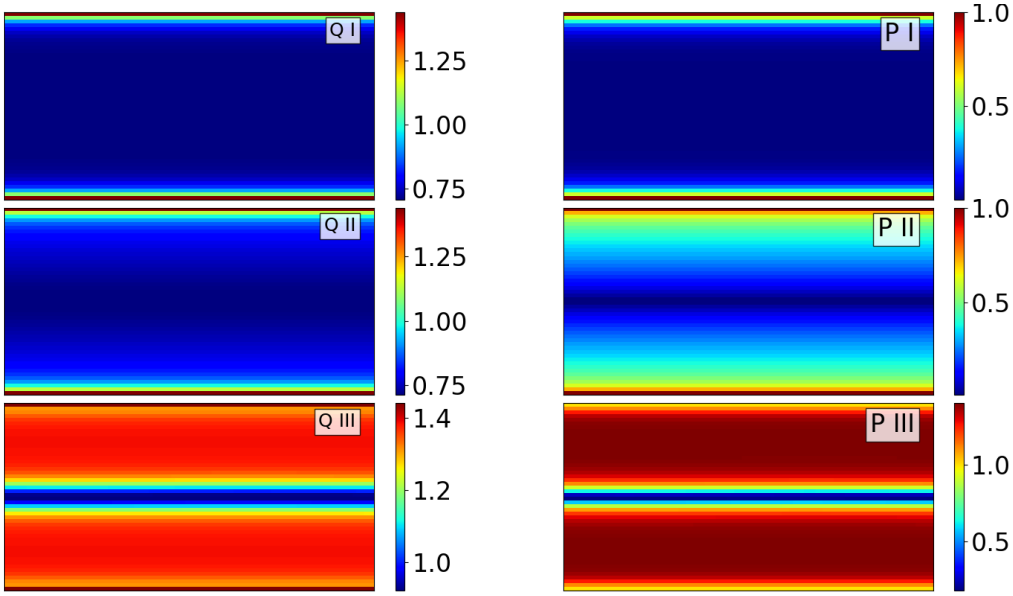


Fig. 5.7 Comparison of nematic order parameters and polarization fields across different $\gamma$ values. Each row of subplots presents data from three different folders, corresponding to $\gamma = 0.00$, 0.60, and 1.00. The left column shows the nematic order parameter (Q) with Roman numerals Q I, Q II, and Q III indicating different states of the nematic order. The right column illustrates the polarization fields (P) for the same $\gamma$ values, with Roman numerals P I, P II, and P III representing different polarization states. Each plot uses the jet colormap to visualize the variation in order parameter and polarization fields. Color bars to the right of each subplot indicate the range of values.

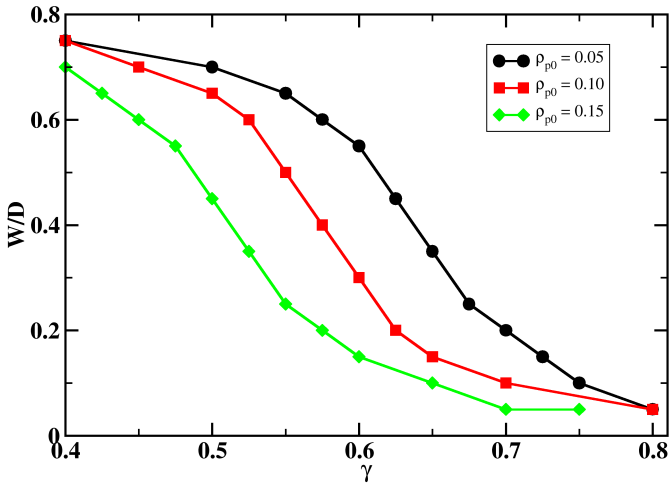


Fig. 5.8 The figure illustrates the plot of width $\frac{W}{D}$ vs coupling strength $\gamma$ for three values of average density of polar particles $\rho_p = (0.05, 0.10, 0.15)$.

## 5.5 Conclusion

We study the effect of polar impurities in liquid crystal system by tuning the coupling strength $\gamma$ and average density of polar particles $\rho_{p0}$. We take the coarse-grained route by simulating the TDGL equations for order parameters $\vec{P}$ and $Q$. For $\gamma = 0$, no string formation is observed. As $\gamma$ increases beyond a optimal value, strings begin to form between defect pairs. The width of these strings decreases with increasing $\gamma$. These strings are visible in the order parameter field of both polar and nematic particles. For polar particles, the magnitude of the order parameter is close to zero along the string, acting as a domain wall separating oppositely oriented domains. Strings are observed to connect two defects regardless of their charge i.e. defect pairs connected through strings can be of the same type (+1/2, +1/2 or -1/2, -1/2) as well as opposite (+1/2, -1/2). Higher densities and stronger coupling result in narrower strings, highlighting the importance of these parameters in determining the system's structural properties.

Further, the trajectory and dynamics of defects are studied by putting the artificial defects in system. The evolution of the system from random and polar order initial conditions reveals that increasing $\gamma$ leads to enhanced dynamics of the defects.

In summary, this study provides a comprehensive analysis of the behavior of topological defects and string formation in coupled polar and nematic systems. The findings reveal the critical role of coupling strength and particle density in determining the structural and

dynamical properties of the system, offering valuable insights into the complex interactions in active matter systems.

**********